

DIFFUSION-BASED EXTREME IMAGE COMPRESSION WITH COMPRESSED FEATURE INITIALIZATION

Zhiyuan Li¹, Yanhui Zhou¹, Hao Wei¹, Chenyang Ge^{1,✉}, Ajmal Mian²

¹Institute of Artificial Intelligence and Robotics, Xi'an Jiaotong University

²Department of Computer Science and Software Engineering, The University of Western Australia
 {lizhiyuan2839@stu, zhouyh@mail, haowei@stu, cyge@mail}.xjtu.edu.cn
 ajmal.mian@uwa.edu.au

ABSTRACT

Diffusion-based extreme image compression methods have achieved impressive performance at extremely low bitrates. However, constrained by the iterative denoising process that starts from pure noise, these methods are limited in both fidelity and efficiency. To address these two issues, we present **Relay Residual Diffusion Extreme Image Compression (RDEIC)**, which leverages compressed feature initialization and residual diffusion. Specifically, we first use the compressed latent features of the image with added noise, instead of pure noise, as the starting point to eliminate the unnecessary initial stages of the denoising process. Second, we design a novel relay residual diffusion that reconstructs the raw image by iteratively removing the added noise and the residual between the compressed and target latent features. Notably, our relay residual diffusion network seamlessly integrates pre-trained stable diffusion to leverage its robust generative capability for high-quality reconstruction. Third, we propose a fixed-step fine-tuning strategy to eliminate the discrepancy between the training and inference phases, further improving the reconstruction quality. Extensive experiments demonstrate that the proposed RDEIC achieves state-of-the-art visual quality and outperforms existing diffusion-based extreme image compression methods in both fidelity and efficiency. The source code will be provided in <https://github.com/huai-chang/RDEIC>.

1 INTRODUCTION

Extreme image compression is becoming increasingly important with the growing demand for efficient storage and transmission of images where storage capacity or bandwidth is limited, such as in satellite communications and mobile devices. Conventional compression standards like JPEG (Wallace, 1991), BPG (Bellard, 2014) and VVC (Bross et al., 2021) rely on hand-crafted rules and block-based redundancy removal techniques, leading to severe blurring and blocking artifacts at low bitrates. Hence, there is an urgent need to explore extreme image compression methods.

In recent years, learned image compression methods have attracted significant interest, outperforming conventional codecs. However, distortion-oriented learned compression methods (Xie et al., 2021; Zhu et al., 2021; Liu et al., 2023; Li et al., 2024a) optimize for the rate-distortion function alone, resulting in unrealistic reconstructions at low bitrates, typically manifested as blurring or over-smoothing. Perceptual-oriented learned compression methods (Agustsson et al., 2019; Mentzer et al., 2020; Muckley et al., 2023; Yang & Mandt, 2023) introduce generative models, such as generative adversarial networks (GANs) (Goodfellow et al., 2014) and diffusion models (Ho et al., 2020), to enhance the perceptual quality of reconstructions. However, these methods are optimized for medium to high bitrates instead of extremely low bitrates such as below 0.1 bpp. As a result, these methods experience significant quality degradation when the compression ratio is increased.

Recently, diffusion-based extreme image compression methods (Lei et al., 2023; Careil et al., 2024; Li et al., 2024b) leverage the robust generative ability of pre-trained text-to-image (T2I) diffusion models, achieving superior visual quality at extremely low bitrates. Nonetheless, these methods are constrained by the inherent characteristics of diffusion models. Firstly, these methods rely on an iter-

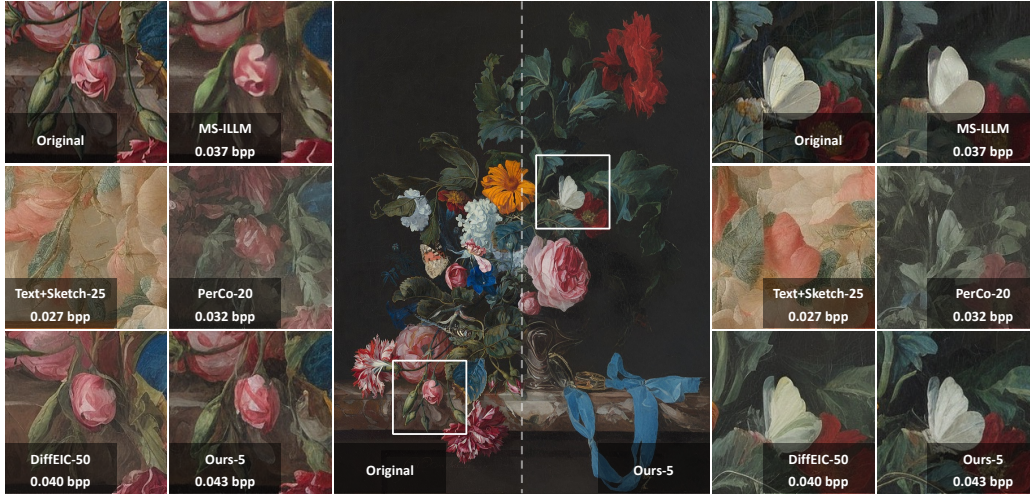


Figure 1: Qualitative comparison between the proposed RDEIC and recent state-of-the-art methods: MS-ILLM (Muckley et al., 2023), Text+Sketch (Lei et al., 2023), PerCo (Careil et al., 2024), and DiffeIC (Li et al., 2024b). For diffusion-based methods, the number of denoising steps is written after the name, e.g. PerCo-20 and Ours-5 means 20 diffusion steps are used by PerCo and 5 diffusion steps are used by our method.

ative denoising process to reconstruct raw images from pure noise which is inefficient for inference (Li et al., 2024b). Secondly, initiating the denoising process from pure noise introduces significant randomness, compromising the fidelity of the reconstructions (Careil et al., 2024). Thirdly, there is a discrepancy between the training and inference phases. During training, each time-step is trained independently, which is well-suited for image generation tasks where diversity (or randomness) is encouraged (Ho et al., 2020). However, this training approach is not optimal for image compression where consistency between the reconstruction and the raw image is crucial.

In this work, we propose **Relay Residual Diffusion Extreme Image Compression (RDEIC)** to overcome the three limitations mentioned above. To overcome the first two limitations, inspired by Relay Diffusion (Teng et al., 2024), we use the compressed latent features with added noise as the starting point, which significantly reduces the number of denoising steps required for reconstruction and enhances the reconstruction fidelity since providing a better starting point. We also propose a novel relay residual diffusion process that reconstructs the raw image by iteratively removing the added noise and the residual between the compressed and target latent features (i.e., the features of the raw image in the latent diffusion space). Furthermore, we integrate pre-trained stable diffusion into our compression framework to leverage its robust generative capability for high perceptual reconstruction. To address the third limitation, we introduce a fixed-step fine-tuning strategy to eliminate the discrepancy between the training and inference phases. By fine-tuning RDEIC throughout the entire reconstruction process, we further improve the reconstruction quality. Moreover, to meet users' diverse requirements, we introduce a controllable detail generation method that achieves a trade-off between smoothness and sharpness by adjusting the intensity of high-frequency components in the reconstructions. As shown in Fig. 1, the proposed RDEIC achieves state-of-the-art perceptual performance at extremely low bitrates, and significantly outperforms existing diffusion-based extreme image compression methods with fewer inference steps.

In summary, our contributions are as follows:

- We propose RDEIC, a novel diffusion model for extreme image compression that accelerates the denoising process through compressed feature initialization i.e. the compressed latent features with added noise, instead of pure noise, are used as the starting point of reverse diffusion.
- We propose a relay residual diffusion process that seamlessly integrates pre-trained stable diffusion into our compression network and removes the residual between the compressed and target latent features.

- To eliminate the discrepancy between the training and inference phases, we design a fixed-step fine-tuning strategy that refines the model through the entire reconstruction process, further improving reconstruction quality.

2 RELATED WORK

Learned Image Compression. As a pioneer work, Ballé et al. (2017) proposed an end-to-end image compression framework to jointly optimize the rate-distortion performance. Ballé et al. (2018) later introduced a hyperprior to reduce spatial dependencies in the latent representation, greatly enhancing performance. Subsequent works further improved compression models by developing various nonlinear transforms (Xie et al., 2021; He et al., 2022; Liu et al., 2023; Li et al., 2024a) and entropy models (Minnen et al., 2018; Minnen & Singh, 2020; He et al., 2021; Qian et al., 2021). However, optimization for rate-distortion alone often results in unrealistic reconstructions at low bitrates, typically manifested as blurring or over-smoothness (Blau & Michaeli, 2019). To improve perceptual quality, generative models have been integrated into compression methods. Agustsson et al. (2019) added an adversarial loss for lost details generation. Mentzer et al. (2020) explored the generator and discriminator architectures, as well as training strategies for perceptual image compression. Muckley et al. (2023) introduced a local adversarial discriminator to enhance statistical fidelity. With the advancement of diffusion models, some efforts have been made to apply diffusion models to image compression. For instance, Yang & Mandt (2023) innovatively introduced a conditional diffusion model as decoder for image compression. Kuang et al. (2024) proposed a consistency guidance architecture to guide the diffusion model in stably reconstructing high-quality images.

Extreme Image Compression. In recent years, extreme image compression has garnered increasing attention, aiming to compress image to extremely low bitrates, often below 0.1 bpp, while maintaining visually acceptable image quality. Gao et al. (2023) leveraged the information-lossless property of invertible neural networks to mitigate the significant information loss in extreme image compression. Jiang et al. (2023) treated text descriptions as prior to ensure semantic consistency between the reconstructions and the raw images. Wei et al. (2024) achieved extreme image compression by rescaling images using extreme scaling factors. Lu et al. (2024) combined continuous and codebook-based discrete features to reconstruct high-quality images at extremely low bitrates. Inspired by the great success of T2I diffusion models in various image restoration tasks (Lin et al., 2023; Wang et al., 2024), some methods have incorporated T2I diffusion models into extreme image compression frameworks. Lei et al. (2023) utilized a pre-trained ControlNet (Zhang et al., 2023) to reconstruct images based on corresponding short text prompts and binary contour sketches. Careil et al. (2024) conditioned iterative diffusion models on vector-quantized latent image representations and textual image descriptions. Li et al. (2024b) combined compressive VAEs with pre-trained T2I diffusion models to achieve realistic reconstructions at extremely low bitrates. However, constrained by the inherent characteristics of diffusion models, these diffusion-based extreme image compression methods are limited in both fidelity and efficiency. In this paper, we propose a solution to these limitations through a relay residual diffusion framework and a fixed-step fine-tuning strategy.

Relay Diffusion. Conventional diffusion models, such as denoising diffusion probabilistic models (DDPM) (Ho et al., 2020) and its variants, operate by progressively adding and removing Gaussian noise through a multi-step Markov process. These models have achieved remarkable results in low-resolution scenarios but face substantial challenges in terms of computational efficiency and performance when applied to higher resolutions. To overcome this, cascaded diffusion methods (Ho et al., 2022; Saharia et al., 2022) are introduced, which decompose the image generation into multiple stages, with each stage responsible for super-resolution conditioning on the previous one. However, these methods still require complete resampling at each stage, leading to inefficiencies and potential mismatches among different resolutions. Relay diffusion, as proposed by Teng et al. (2024), extends the cascaded framework by continuing the diffusion process directly from the low-resolution output rather than restarting from pure noise, which allows the higher-resolution stages to correct artifacts from earlier stages. This design is particularly well-suited for extreme image compression tasks where compressed latent features of the raw image are available. Therefore, we propose a novel relay residual diffusion process that integrates relay diffusion with diffusion-based extreme image compression method, greatly enhancing reconstruction efficiency and fidelity at extremely low bitrates.

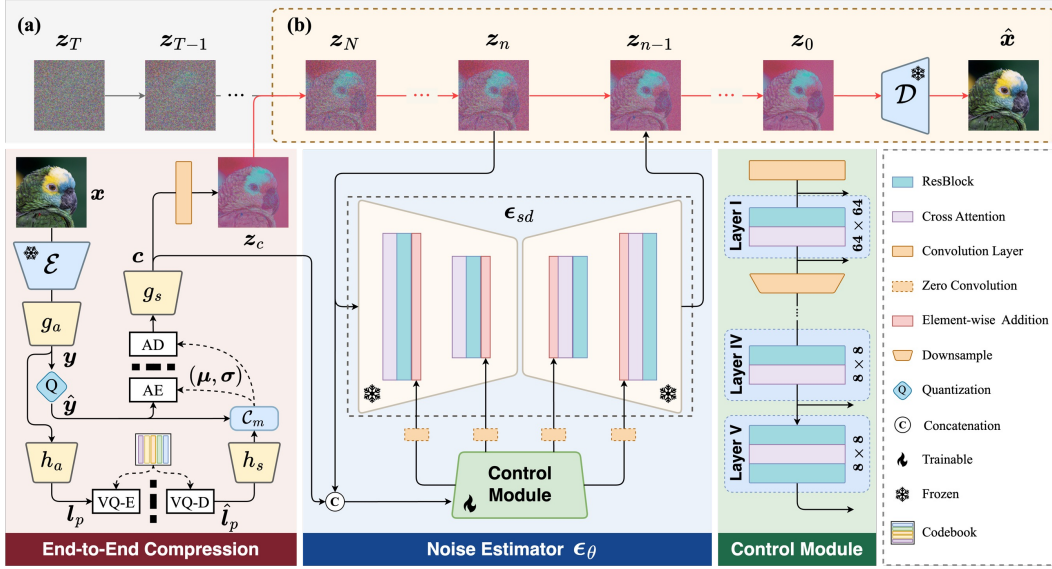


Figure 2: The proposed RDEIC. We first map a raw image x into the latent space using the encoder \mathcal{E} and then perform end-to-end lossy compression to get compressed latent features z_c . We then use z_c with added noise as the starting point and apply a denoising process to reconstruct the noise-free latent feature z_0 . The decoder \mathcal{D} maps z_0 back to the pixel space, to get the reconstructed image \hat{x} . (a) Vanilla diffusion framework that starts from pure noise. (b) The proposed relay residual diffusion framework that starts from compressed latent features with added noise.

3 METHODOLOGY

3.1 OVERALL FRAMEWORK

Fig. 2 shows an overview of the proposed RDEIC network. We first use an encoder \mathcal{E} and analysis transform g_a to convert the input image x to its latent representation y . Then we perform hyper transform coding on y with the categorical hyper model (Jia et al., 2024) and use the space-channel context model \mathcal{C}_m to predict the entropy parameters (μ, σ) to estimate the distribution of quantized latent representation \hat{y} (He et al., 2022). Subsequently, the synthesis transform g_s is used to obtain the image content dependent features z_c . Random noise is then added to z_c , which is the starting point for reconstructing the noise-free latent features z_0 through an iterative denoising process. The denoising process is implemented by a frozen pre-trained noise estimator ϵ_{sd} of stable diffusion with trainable control network for intermediate feature modulation. Finally, the reconstructed image \hat{x} is decoded from z_0 using the decoder \mathcal{D} .

3.2 ACCELERATING DENOISING PROCESS WITH RELAY RESIDUAL DIFFUSION

Following stable diffusion, existing diffusion-based extreme image compression methods obtain the noisy latent by adding Gaussian noise with variance $\beta_t \in (0, 1)$ to the noise-free latent features z_0 :

$$z_t = \sqrt{\bar{\alpha}_t} z_0 + \sqrt{1 - \bar{\alpha}_t} \epsilon_t, \quad t = 1, 2, \dots, T, \quad (1)$$

where $\epsilon_t \sim \mathcal{N}(0, \mathbf{I})$, $\alpha_t = 1 - \beta_t$ and $\bar{\alpha}_t = \prod_{i=1}^t \alpha_i$. When t is large enough, the noisy latent z_t is nearly a standard Gaussian distribution. In practice, T is typically very large, e.g., 1000, and pure noise is set as the starting point for the reverse diffusion process. However, this approach is not optimal for the image compression task, where the compressed latent features z_c are available.

To this end, we set the starting point to $z_N = \sqrt{\bar{\alpha}_N} z_c + \sqrt{1 - \bar{\alpha}_N} \epsilon_N$, where $N \ll T$. Our relay residual diffusion is thus defined as:

$$z_n = \sqrt{\bar{\alpha}_n} (z_0 + \eta_n e) + \sqrt{1 - \bar{\alpha}_n} \epsilon_n, \quad n = 1, 2, \dots, N, \quad (2)$$

where e denotes the residual between z_c and z_0 , i.e., $e = z_c - z_0$, and $\{\eta_n\}_{n=1}^N$ is a weight sequence that satisfies $\eta_1 \rightarrow 0$ and $\eta_N = 1$. Since the residual e is unavailable during inference, we refer to DDIM (Song et al., 2021) and assume that z_{n-1} is a linear combination of z_n and z_0 :

$$z_{n-1} = k_n z_0 + m_n z_n + \sigma_n \epsilon, \quad (3)$$

where we set $\sigma_n = 0$ for simplicity. Combining Eq. (2) and Eq. (3), we get

$$\frac{\eta_n}{\eta_{n-1}} = \frac{\sqrt{1 - \bar{\alpha}_n}/\sqrt{\bar{\alpha}_n}}{\sqrt{1 - \bar{\alpha}_{n-1}}/\sqrt{\bar{\alpha}_{n-1}}} \rightarrow \eta_n = \lambda \frac{\sqrt{1 - \bar{\alpha}_n}}{\sqrt{\bar{\alpha}_n}}, \quad (4)$$

where we set $\lambda = \frac{\sqrt{\bar{\alpha}_N}}{\sqrt{1 - \bar{\alpha}_N}}$ to ensure $\eta_N = 1$. Detailed derivation is presented in Appendix A. Substituting Eq. (4) into Eq. (2), the diffusion process can be further written as follows:

$$z_n = \sqrt{\bar{\alpha}_n}(z_0 + \lambda \frac{\sqrt{1 - \bar{\alpha}_n}}{\sqrt{\bar{\alpha}_n}} e) + \sqrt{1 - \bar{\alpha}_n} \epsilon_n \quad (5)$$

$$= \sqrt{\bar{\alpha}_n} z_0 + \sqrt{1 - \bar{\alpha}_n} \underbrace{(\lambda e + \epsilon_n)}_{\tilde{\epsilon}_n}. \quad (6)$$

Since Eq. (6) has the same structure as Eq. (1), we can easily incorporate stable diffusion into our framework. For the denoising process, the noise estimator ϵ_θ is learned to predict $\tilde{\epsilon}_n$ at each time-step n . The optimization of noise estimator ϵ_θ is defined as

$$\mathcal{L}_{ne} = \mathbb{E}_{z_0, z_c, e, n, \epsilon_n} \|z_0 - \hat{z}_0\|_2^2 \quad (7)$$

$$= \omega_n \mathbb{E}_{z_0, z_c, e, n, \epsilon_n} \|\tilde{\epsilon}_n - \epsilon_\theta(z_n, c, n)\|_2^2, \quad (8)$$

where $\omega_n = \frac{1 - \bar{\alpha}_n}{\bar{\alpha}_n}$. After that, we can start from the compressed latent features z_c and reconstruct the image using Eq. 3 without knowing the residual e .

3.3 FIXED-STEP FINE-TUNING STRATEGY

Most existing diffusion-based image compression methods adopt the same training strategy as DDPM (Ho et al., 2020), where each time-step is trained independently. However, the lack of coordination among time-steps can lead to error accumulation and suboptimal reconstruction quality. To address this issue, we employ a two-stage training strategy. As shown in Fig. 3(a), we first train each time-step n independently, allowing the model to learn to remove noise and residuals at each step. The optimization objective consists of the rate-distortion loss, codebook loss (Van Den Oord et al., 2017) and noise estimation loss:

$$\mathcal{L}_{stage I} = \underbrace{\lambda_r \|z_0 - z_c\|_2^2 + R(\hat{y})}_{\text{rate-distortion loss } \mathcal{L}_{rd}} + \underbrace{\|sg(\hat{t}_p) - \hat{t}_p\|_2^2 + \beta \|sg(\hat{t}_p) - t_p\|_2^2}_{\text{codebook loss } \mathcal{L}_{cb}} + \lambda_r \mathcal{L}_{ne}, \quad (9)$$

where λ_r is the hyper-parameter that controls the trade-off, $R(\cdot)$ denotes the estimated rate, $sg(\cdot)$ denotes the stop-gradient operator, and $\beta = 0.25$. Thanks to the proposed relay residual diffusion framework, we can achieve high-quality reconstruction in fewer than 5 denoising steps, as demonstrated in Fig. 6. This efficiency allows us to fine-tune the model using the entire reconstruction process with limited computational resources.

To this end, we further employ a fixed-step fine-tuning strategy to eliminate the discrepancy between the training and inference phases. As shown in Fig. 3(b), in each training step, we utilize spaced DDPM sampling (Nichol & Dhariwal, 2021) with L fixed time-steps to reconstruct the noise-free latent features \hat{z}_0 from the starting point z_N and map \hat{z}_0 back to the pixel space $\hat{x} = \mathcal{D}(\hat{z}_0)$. The loss function used in this stage is as follows:

$$\mathcal{L}_{stage II} = \mathcal{L}_{rd} + \mathcal{L}_{cb} + \lambda_r \|z_0 - \hat{z}_0\|_2^2 + \lambda_r (\|\mathbf{x} - \hat{\mathbf{x}}\|_2^2 + \lambda_{l_{lips}} \mathcal{L}_{lips}(\mathbf{x}, \hat{\mathbf{x}})), \quad (10)$$

where \mathcal{L}_{lips} denotes the LPIPS loss and $\lambda_{lips} = 0.5$ is the weight of the LPIPS loss. By fine-tuning the model using the entire reconstruction process, we achieve significant performance improvement.

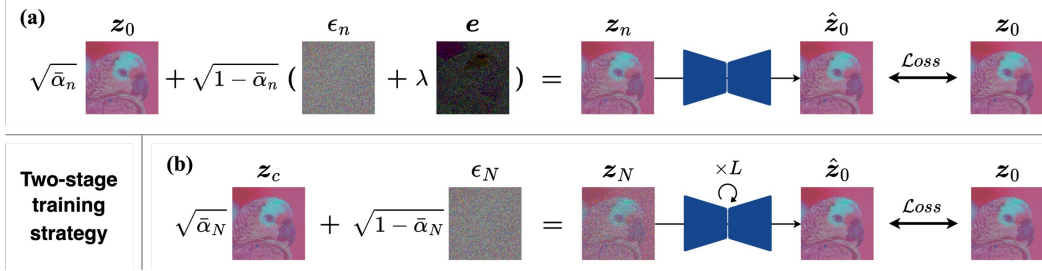


Figure 3: The two-stage training strategy of RDEIC. (a) Independent training: we randomly pick a time-step n and train each time-step n independently. This ensures that the model effectively learns to remove added noise and residuals at every step. (b) Fixed-step fine-tuning: L fixed denoising steps are used to iteratively reconstruct a noise-free latent features \hat{z}_0 from z_N , which is consistent with the inference phase.

3.4 CONTROLLABLE DETAIL GENERATION

Although the fixed-step fine-tuning strategy significantly improves reconstruction quality, it requires a fixed number of denoising steps in the inference phase, making it impossible to achieve a trade-off between smoothness and sharpness by adjusting the number of denoising steps (Li et al., 2024b). To address this limitation, we introduce a controllable detail generation method that allows us to dynamically balance smoothness and sharpness without being constrained by the fixed-step requirement, which enables more versatile and user-specific image reconstructions.

Since the compressed latent feature already contains image information, directly using stable diffusion’s noise estimator ϵ_{sd} to predict noise $\epsilon_{sd}(z_n, n)$ results in low-frequency reconstructed images, as shown in the second column of Fig. 7 and Fig. 13. Inspired by classifier-free guidance (Ho & Salimans, 2021), we decompose the predicted noise $\epsilon_\theta(z_n, c, n)$ into a low-frequency component $\epsilon_{sd}(z_n, n)$ and a high-frequency component $\epsilon_\theta(z_n, c, n) - \epsilon_{sd}(z_n, n)$, and control the balance between smoothness and sharpness by adjusting the intensity of the high-frequency component:

$$\hat{\epsilon}_n = \epsilon_{sd}(z_n, n) + \lambda_s(\epsilon_\theta(z_n, c, n) - \epsilon_{sd}(z_n, n)), \quad (11)$$

where λ_s is the guidance scale. By adjusting the value of λ_s , we can regulate the amount of high-frequency details introduced into the reconstructed image.

4 EXPERIMENTS

4.1 EXPERIMENTAL SETUP

Datasets. The proposed RDEIC is trained on the **LSDIR** (Li et al., 2023) dataset, which contains 84,911 high-quality images. For evaluation, we use three common benchmark datasets, i.e., the **Kodak** (Franzen, 1999) dataset with 24 natural images of 768×512 pixels, the **Tecnick** (Asuni & Giachetti, 2014) dataset with 140 images of 1200×1200 pixels, and the **CLIC2020** (Toderici et al., 2020) dataset with 428 high-quality images. For the Tecnick and CLIC2020 datasets, we resize the images so that the shorter dimension is equal to 768 and then center-crop them with 768×768 spatial resolution (Yang & Mandt, 2023).

Implementation details. For training, we use the Adam (Kingma & Ba, 2014) optimizer with $\beta_1 = 0.9$ and $\beta_2 = 0.999$ for a total of 300K iterations. The batch size is set to 4. We use Stable Diffusion 2.1-base¹ as the specific implementation of stable diffusion. Throughout all our experiments, the weights of stable diffusion remain frozen. To achieve different compression ratios, we train five models with λ_r selected from $\{2, 1, 0.5, 0.25, 0.1\}$. The total number N of denoising steps is set to 300. As described in Section 3.3, the training process is divided into two stages. 1) *Independent training.* During this stage, the initial learning rate is set to 1×10^{-4} and images are randomly cropped to 512×512 patches. We first train the proposed RDEIC with $\lambda_r = 2$ for 100K

¹<https://huggingface.co/stabilityai/stable-diffusion-2-1-base>

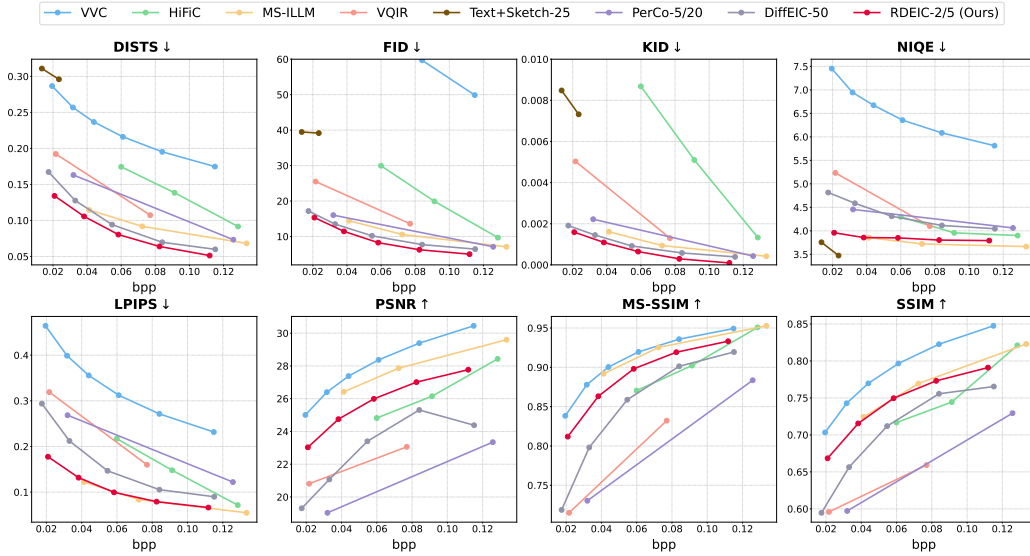


Figure 4: Quantitative comparisons with state-of-the-art methods on the CLIC2020 dataset.

Table 1: BD-rate (%) for different methods on the CLIC2020 dataset.

Methods	Perception					Distortion			Average
	DISTS	FID	KID	NIQE	LPIPS	PSNR	MS-SSIM	SSIM	
HiFiC	241.7	261.9	404.6	349.3	137.4	41.1	39.5	53.6	161.9
VQIR	122.7	198.3	185.1	188.2	199.4	263.0	182.7	334.5	219.4
MS-ILLM	50.7	71.2	71.7	-38.4	-4.8	-37.3	-22.4	-6.0	4.1
PerCo	104.0	104.7	98.9	524.5	216.8	433.8	171.5	188.6	237.2
DiffeIC	21.9	22.4	28.3	514.6	68.9	158.1	48.7	48.5	108.2
RDEIC (Ours)	0	0	0	0	0	0	0	0	0

iterations. The learning rate is then reduced to 2×10^{-5} and the model is trained with target λ_r for another 100K iterations. 2) *Fixed-step fine-tuning*. In this stage, the learning rate is set to 2×10^{-5} and images are randomly cropped to 256×256 patches. We fine-tune the model through the entire reconstruction process for 100K iterations. When $\lambda_r \in \{2, 1\}$, the fixed number L is set to 2, otherwise, it is 5. All experiments are conducted on a single NVIDIA GeForce RTX 4090 GPU.

Metrics. For quantitative evaluation, we employ several established metrics to measure the visual quality of the reconstructed images, including reference perceptual metrics **LPIPS** (Zhang et al., 2018), **DISTS** (Ding et al., 2020), **FID** (Heusel et al., 2017) and **KID** (Bińkowski et al., 2018) and no-reference perceptual metrics **NIQE** (Mittal et al., 2012). We also employ distortion metrics **PSNR**, **SSIM** and **MS-SSIM** (Wang et al., 2003) to measure the fidelity of reconstructions. Note that FID and KID are calculated on 256×256 patches according to Mentzer et al. (2020).

Comparison methods. We compare the proposed RDEIC with several representative extreme image compression methods, including the traditional compression standard: VVC (Bross et al., 2021); GANs-based compression methods: HiFiC (Mentzer et al., 2020), MS-ILLM (Muckley et al., 2023), and VQIR (Wei et al., 2024), and diffusion-based methods: Text+Sketch (Lei et al., 2023), PerCo (Careil et al., 2024), and DiffeIC (Li et al., 2024b). More details can be found in Appendix B.

4.2 EXPERIMENTAL RESULTS

Quantitative comparisons. Fig. 4 shows the performance of the proposed and compared methods on the CLIC2020 dataset. It can be observed that the proposed RDEIC demonstrates superior performance across different perceptual metrics compared to other methods, particularly achieving

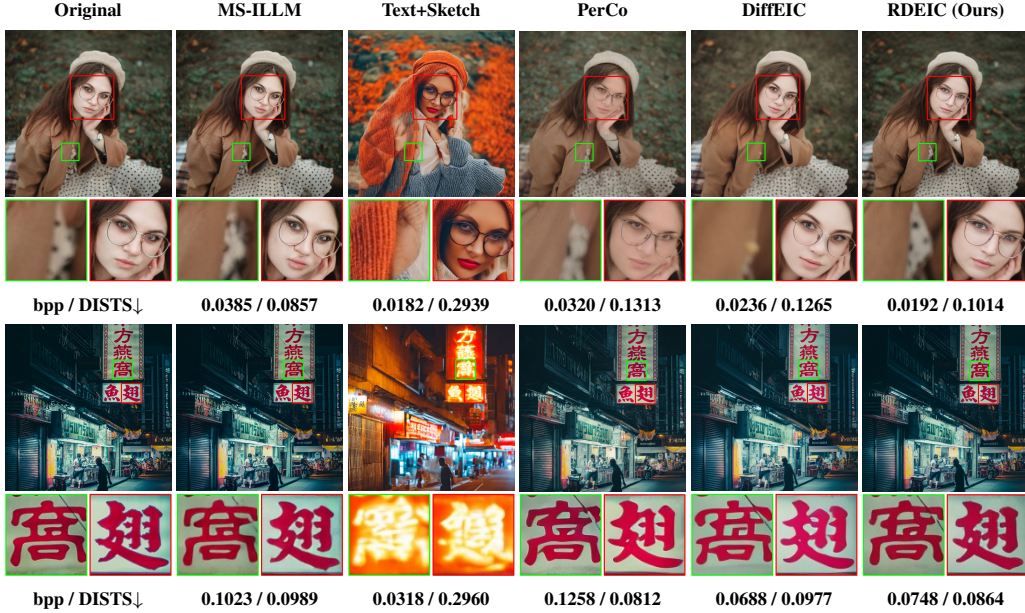


Figure 5: Visual comparisons of our method to baselines on the CLIC2020 dataset. The bpp and DISTs of each method are shown at the bottom of each image. Compared to other methods, our method produces more realistic and faithful reconstructions.

optimal results in DISTs, FID, and KID. For the distortion metrics, RDEIC significantly outperforms other diffusion-based methods, underscoring its superiority in maintaining consistency. To provide a more intuitive comparison of overall performance, we set our method as the anchor and compute the BD-rate (Bjontegaard, 2001) for each metric. The results are shown in Table 1. We observe that our method outperforms all the comparison methods, where the average BD-rate values of the competing methods are positive. In addition, the comparison results on the Tecnick and Kodak datasets are shown in Fig. 9 and Fig. 10, respectively, in Appendix C.

Qualitative comparisons. Fig. 5 provides visual comparisons among the evaluated methods at extremely low bitrates. MS-ILLM (Muckley et al., 2023) excels at reconstructing structural information, such as text, but falls significantly short in preserving textures and fine details. Diffusion-based Text+Sketch (Lei et al., 2023), PerCo (Careil et al., 2024) and DiffeIC (Li et al., 2024b) achieve realistic reconstruction at extremely low bitrates but often generate details and structures that are inconsistent with the original image. In comparison, the proposed RDEIC produces reconstructions with higher visual quality, fewer artifacts, and more faithful details. More visualization results can be found in Fig. 11 and Fig. 12 in Appendix C.

Complexity comparisons. Table 2 summarizes the average encoding/decoding times along with standard deviations for different methods on the Kodak dataset. Similar to PerCo (Careil et al., 2024), our RDEIC uses different denoising steps for different compression ratios. Due to the reliance on an iterative denoising process, diffusion-based extreme image compression methods require more time to reconstruct images than the GAN-based MS-ILLM (Muckley et al., 2023) and VQIR (Wei et al., 2024). Benefiting from the proposed relay residual diffusion, our RDEIC achieves high-quality image reconstruction with fewer denoising steps compared to other diffusion-based methods, significantly reducing the decoding time. For instance, compared to DiffeIC (Li et al., 2024b), our RDEIC is about 7 times faster using 5 denoising steps, and this speed advantage increases to a factor of 12 when using 2 denoising steps.

4.3 ABLATIONS

To provide a more comprehensive analysis of the proposed method, we conduct ablation studies, with the results presented in Table 3. For the baseline, we employ the same diffusion framework as DiffeIC (Li et al., 2024b), where the denoising process starts from pure noise. Due to the inherent

Table 2: Encoding and decoding time (in seconds) on Kodak dataset. BD-rate (%) is calculated on CLIC2020 dataset, with DISTS as the metric. DS denotes denoising steps.

Types	Methods	DS	Encoding Time	Decoding Time	BD-rate (%)
GAN-based	MS-ILLM	–	0.038 ± 0.004	0.059 ± 0.004	50.7
	VQIR	–	0.050 ± 0.003	0.179 ± 0.005	122.7
Diffusion-based	Text+Sketch	25	62.045 ± 0.516	12.028 ± 0.413	12584.9
	PerCo	5	0.236 ± 0.040	0.778 ± 0.007	104.0
	PerCo	20	0.236 ± 0.040	2.670 ± 0.008	104.0
	DiffeIC	50	0.128 ± 0.005	4.574 ± 0.006	21.9
	RDEIC (Ours)	2	0.119 ± 0.003	0.379 ± 0.005	0
	RDEIC (Ours)	5	0.119 ± 0.003	0.643 ± 0.004	0

Table 3: Ablation studies of Relay Residual Diffusion (RRD) framework and Fixed-Step Fine-Tuning (FSFT) strategy. BD-rate is calculated on CLIC2020 dataset. DS denotes denoising steps.

Methods	Starting Point	DS	w/ RRD	w/ FSFT	BD-rate (%)		
					Distortion	Perception	Average
Baseline	$\mathcal{N}(0, I)$	2/5	×	×	209.0	247.0	228.0
		50	×	×	100.9	50.7	75.8
v_1	z_N	2/5	✓	×	27.2	46.4	36.8
RDEIC (Ours)	z_N	2/5	✓	✓	0	0	0

characteristics of diffusion models, the baseline requires a large number of denoising steps to achieve optimal performance and exhibits poor distortion performance.

Effectiveness of relay residual diffusion. We first investigate the effectiveness of our proposed relay residual diffusion framework. As shown in Table 3, incorporating the relay residual diffusion framework significantly decreases the denoising steps required for reconstruction meanwhile achieves better reconstruction quality (v_1 vs. Baseline). Specifically, v_1 uses only 2 or 5 denoising steps, while the baseline requires up to 50 steps to achieve similar perceptual performance, indicating that our relay residual diffusion framework can efficiently remove both added noise and residuals. Moreover, v_1 significantly outperforms the baseline in terms of distortion metrics, demonstrating that its reconstruction results have higher fidelity. The reason behind this is that starting from the compressed latent feature, instead of pure noise, avoids the error accumulation in the initial stage of the denoising process and provides a solid foundation for subsequent detail generation.

Analysis for fixed-step fine-tuning. We further demonstrate the effectiveness of the FSFT strategy. Before doing this, we need to analyze the impact of denoising steps in order to select an appropriate value of L for this strategy. As shown in Fig. 6, for $\lambda_r \in \{2, 1\}$, the number of denoising steps has minimal effect on compression performance, so that we set L to 2 in this case. For $\lambda_r \in \{0.5, 0.25, 0.1\}$, increasing the denoising steps achieves better perceptual results (lower LPIPS and DISTS values), but leads to degraded fidelity (lower PSNR and MS-SSIM values). To achieve a balance between fidelity and perceptual quality, we set L to 5 here. In Table 3, using FSFT can yield bitrate savings of 27.2% and 46.4% in terms of distortion and perception metrics, respectively (v_1 vs. RDEIC).

Smoothness-sharpness trade-off. To fully leverage the generative potential of pre-trained stable diffusion, we introduce a controllable detail generation method that allows users to explore and customize outputs according to their personal preferences. The visualization result is shown in Fig. 7. We control the balance between smoothness and sharpness by adjusting the parameter λ_s , which regulates the amount of high-frequency details introduced into the reconstructed image. Specifically, as the value of λ_s increases, the image transitions from a smooth appearance to a progressively sharper and more detailed reconstruction. Additional results are provided in Fig. 13, Fig. 14, and Fig. 15 in Appendix C.

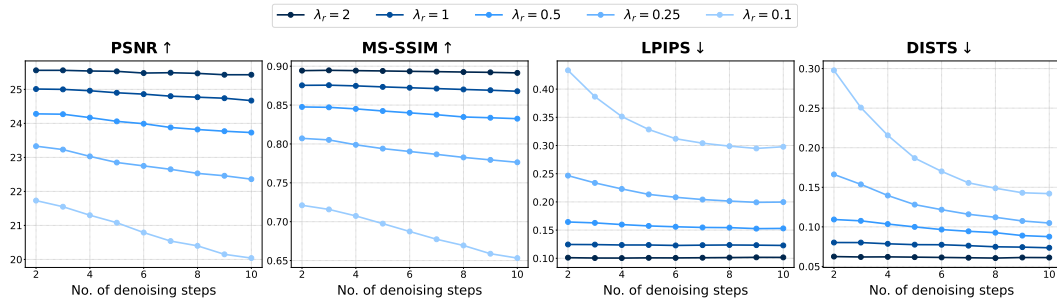


Figure 6: Quantitative comparisons of different number of denoising steps.

Figure 7: Balancing smoothness versus sharpness. The second row shows the absolute difference between the reconstructed images and the baseline ($\lambda_s = 0$).

5 CONCLUSION

In this paper, we propose an innovative relay residual diffusion-based method (RDEIC) for extreme image compression. Unlike most existing diffusion-based methods that start from pure noise, RDEIC takes the compressed latent features of the input image with added noise as the starting point and reconstructs the image by iteratively removing the noise and reducing the residual between the compressed latent features and the target latent features. Extensive experiments have demonstrated the superior performance of our RDEIC over existing state-of-the-art methods in terms of both reconstruction quality and computational complexity.

REFERENCES

- Eirikur Agustsson, Michael Tschannen, Fabian Mentzer, Radu Timofte, and Luc Van Gool. Generative adversarial networks for extreme learned image compression. In *Proceedings of the IEEE/CVF International Conference on Computer Vision*, pp. 221–231, 2019.
- Nicola Asuni and Andrea Giachetti. Testimages: a large-scale archive for testing visual devices and basic image processing algorithms. In *STAG*, pp. 63–70, 2014.
- Johannes Ballé, Valero Laparra, and Eero P Simoncelli. End-to-end optimized image compression. In *5th International Conference on Learning Representations, ICLR 2017*, 2017.
- Johannes Ballé, David Minnen, Saurabh Singh, Sung Jin Hwang, and Nick Johnston. Variational image compression with a scale hyperprior. In *International Conference on Learning Representations*, 2018.
- Fabrice Bellard. Bpg image format. 2014. URL <https://bellard.org/bpg/>.

- Mikołaj Bińkowski, Danica J Sutherland, Michael Arbel, and Arthur Gretton. Demystifying mmd gans. *arXiv preprint arXiv:1801.01401*, 2018.
- Gisle Bjontegaard. Calculation of average psnr differences between rd-curves. *ITU SG16 Doc. VCEG-M33*, 2001.
- Yochai Blau and Tomer Michaeli. Rethinking lossy compression: The rate-distortion-perception tradeoff. In *International Conference on Machine Learning*, pp. 675–685. PMLR, 2019.
- Benjamin Bross, Ye-Kui Wang, Yan Ye, Shan Liu, Jianle Chen, Gary J Sullivan, and Jens-Rainer Ohm. Overview of the versatile video coding (vvc) standard and its applications. *IEEE Transactions on Circuits and Systems for Video Technology*, 31(10):3736–3764, 2021.
- Marlene Careil, Matthew J. Muckley, Jakob Verbeek, and Stéphane Lathuilière. Towards image compression with perfect realism at ultra-low bitrates. In *The Twelfth International Conference on Learning Representations*, 2024. URL <https://openreview.net/forum?id=ktdETU9JBg>.
- Keyan Ding, Kede Ma, Shiqi Wang, and Eero P Simoncelli. Image quality assessment: Unifying structure and texture similarity. *IEEE transactions on pattern analysis and machine intelligence*, 44(5):2567–2581, 2020.
- Rich Franzen. Kodak photocd dataset. 1999. URL <http://r0k.us/graphics/kodak/>.
- Fangyuan Gao, Xin Deng, Junpeng Jing, Xin Zou, and Mai Xu. Extremely low bit-rate image compression via invertible image generation. *IEEE Transactions on Circuits and Systems for Video Technology*, 2023.
- Ian Goodfellow, Jean Pouget-Abadie, Mehdi Mirza, Bing Xu, David Warde-Farley, Sherjil Ozair, Aaron Courville, and Yoshua Bengio. Generative adversarial nets. *Advances in neural information processing systems*, 27, 2014.
- Dailan He, Yaoyan Zheng, Baocheng Sun, Yan Wang, and Hongwei Qin. Checkerboard context model for efficient learned image compression. In *Proceedings of the IEEE/CVF Conference on Computer Vision and Pattern Recognition*, pp. 14771–14780, 2021.
- Dailan He, Ziming Yang, Weikun Peng, Rui Ma, Hongwei Qin, and Yan Wang. Elic: Efficient learned image compression with unevenly grouped space-channel contextual adaptive coding. In *Proceedings of the IEEE/CVF Conference on Computer Vision and Pattern Recognition*, pp. 5718–5727, 2022.
- Martin Heusel, Hubert Ramsauer, Thomas Unterthiner, Bernhard Nessler, and Sepp Hochreiter. Gans trained by a two time-scale update rule converge to a local nash equilibrium. *Advances in neural information processing systems*, 30, 2017.
- Jonathan Ho and Tim Salimans. Classifier-free diffusion guidance. In *NeurIPS 2021 Workshop on Deep Generative Models and Downstream Applications*, 2021. URL <https://openreview.net/forum?id=qw8AKxfYbI>.
- Jonathan Ho, Ajay Jain, and Pieter Abbeel. Denoising diffusion probabilistic models. *Advances in neural information processing systems*, 33:6840–6851, 2020.
- Jonathan Ho, Chitwan Saharia, William Chan, David J Fleet, Mohammad Norouzi, and Tim Salimans. Cascaded diffusion models for high fidelity image generation. *Journal of Machine Learning Research*, 23(47):1–33, 2022.
- Zhaoyang Jia, Jiahao Li, Bin Li, Houqiang Li, and Yan Lu. Generative latent coding for ultra-low bitrate image compression. In *Proceedings of the IEEE/CVF Conference on Computer Vision and Pattern Recognition*, pp. 26088–26098, 2024.
- Xuhao Jiang, Weimin Tan, Tian Tan, Bo Yan, and Liquan Shen. Multi-modality deep network for extreme learned image compression. In *Proceedings of the AAAI Conference on Artificial Intelligence*, volume 37, pp. 1033–1041, 2023.

- Diederik P Kingma and Jimmy Ba. Adam: A method for stochastic optimization. *arXiv preprint arXiv:1412.6980*, 2014.
- Haowei Kuang, Yiyang Ma, Wenhan Yang, Zongming Guo, and Jiaying Liu. Consistency guided diffusion model with neural syntax for perceptual image compression. In *ACM Multimedia*, 2024.
- Eric Lei, Yigit Berkay Uslu, Hamed Hassani, and Shirin Saeedi Bidokhti. Text+ sketch: Image compression at ultra low rates. In *ICML 2023 Workshop Neural Compression: From Information Theory to Applications*, 2023.
- Han Li, Shaohui Li, Wenrui Dai, Chenglin Li, Junni Zou, and Hongkai Xiong. Frequency-aware transformer for learned image compression. In *The Twelfth International Conference on Learning Representations*, 2024a. URL <https://openreview.net/forum?id=HKGQDDTuvZ>.
- Yawei Li, Kai Zhang, Jingyun Liang, Jiezhong Cao, Ce Liu, Rui Gong, Yulun Zhang, Hao Tang, Yun Liu, Denis Demandolx, et al. Lsdir: A large scale dataset for image restoration. In *Proceedings of the IEEE/CVF Conference on Computer Vision and Pattern Recognition*, pp. 1775–1787, 2023.
- Zhiyuan Li, Yanhui Zhou, Hao Wei, Chenyang Ge, and Jingwen Jiang. Towards extreme image compression with latent feature guidance and diffusion prior. *IEEE Transactions on Circuits and Systems for Video Technology*, 2024b.
- Xinqi Lin, Jingwen He, Ziyang Chen, Zhaoyang Lyu, Ben Fei, Bo Dai, Wanli Ouyang, Yu Qiao, and Chao Dong. Diffbir: Towards blind image restoration with generative diffusion prior. *arXiv preprint arXiv:2308.15070*, 2023.
- Jinming Liu, Heming Sun, and Jiro Katto. Learned image compression with mixed transformer-cnn architectures. In *Proceedings of the IEEE/CVF Conference on Computer Vision and Pattern Recognition*, pp. 14388–14397, 2023.
- Lei Lu, Yanyue Xie, Wei Jiang, Wei Wang, Xue Lin, and Yanzhi Wang. Hybridflow: Infusing continuity into masked codebook for extreme low-bitrate image compression. In *ACM Multimedia 2024*, 2024. URL <https://openreview.net/forum?id=jwuX7LktIH>.
- Fabian Mentzer, George D Toderici, Michael Tschannen, and Eirikur Agustsson. High-fidelity generative image compression. *Advances in Neural Information Processing Systems*, 33:11913–11924, 2020.
- David Minnen and Saurabh Singh. Channel-wise autoregressive entropy models for learned image compression. In *2020 IEEE International Conference on Image Processing (ICIP)*, pp. 3339–3343. IEEE, 2020.
- David Minnen, Johannes Ballé, and George D Toderici. Joint autoregressive and hierarchical priors for learned image compression. *Advances in neural information processing systems*, 31, 2018.
- Anish Mittal, Rajiv Soundararajan, and Alan C Bovik. Making a “completely blind” image quality analyzer. *IEEE Signal processing letters*, 20(3):209–212, 2012.
- Matthew J Muckley, Alaaeldin El-Nouby, Karen Ullrich, Hervé Jégou, and Jakob Verbeek. Improving statistical fidelity for neural image compression with implicit local likelihood models. In *International Conference on Machine Learning*, pp. 25426–25443. PMLR, 2023.
- Alexander Quinn Nichol and Prafulla Dhariwal. Improved denoising diffusion probabilistic models. In *International conference on machine learning*, pp. 8162–8171. PMLR, 2021.
- Yichen Qian, Xiuyu Sun, Ming Lin, Zhiyu Tan, and Rong Jin. Entroformer: A transformer-based entropy model for learned image compression. In *International Conference on Learning Representations*, 2021.
- Chitwan Saharia, William Chan, Saurabh Saxena, Lala Li, Jay Whang, Emily L Denton, Kamyar Ghasemipour, Raphael Gontijo Lopes, Burcu Karagol Ayan, Tim Salimans, et al. Photorealistic text-to-image diffusion models with deep language understanding. *Advances in neural information processing systems*, 35:36479–36494, 2022.

- Jiaming Song, Chenlin Meng, and Stefano Ermon. Denoising diffusion implicit models. In *International Conference on Learning Representations*, 2021. URL <https://openreview.net/forum?id=St1giarCHLP>.
- Jiayan Teng, Wendi Zheng, Ming Ding, Wenyi Hong, Jianqiao Wangni, Zhuoyi Yang, and Jie Tang. Relay diffusion: Unifying diffusion process across resolutions for image synthesis. In *The Twelfth International Conference on Learning Representations*, 2024. URL <https://openreview.net/forum?id=qTlcbLSm4p>.
- George Toderici, Lucas Theis, Nick Johnston, Eirikur Agustsson, Fabian Mentzer, Johannes Ballé, Wenzhe Shi, and Radu Timofte. Clic 2020: Challenge on learned image compression, 2020.
- Aaron Van Den Oord, Oriol Vinyals, et al. Neural discrete representation learning. *Advances in neural information processing systems*, 30, 2017.
- Gregory K Wallace. The jpeg still picture compression standard. *Communications of the ACM*, 34(4):30–44, 1991.
- Jianyi Wang, Zongsheng Yue, Shangchen Zhou, Kelvin CK Chan, and Chen Change Loy. Exploiting diffusion prior for real-world image super-resolution. *International Journal of Computer Vision*, pp. 1–21, 2024.
- Zhou Wang, Eero P Simoncelli, and Alan C Bovik. Multiscale structural similarity for image quality assessment. In *The Thirty-Seventh Asilomar Conference on Signals, Systems & Computers, 2003*, volume 2, pp. 1398–1402. Ieee, 2003.
- Hao Wei, Chenyang Ge, Zhiyuan Li, Xin Qiao, and Pengchao Deng. Towards extreme image rescaling with generative prior and invertible prior. *IEEE Transactions on Circuits and Systems for Video Technology*, 2024.
- Yueqi Xie, Ka Leong Cheng, and Qifeng Chen. Enhanced invertible encoding for learned image compression. In *Proceedings of the 29th ACM international conference on multimedia*, pp. 162–170, 2021.
- Ruihan Yang and Stephan Mandt. Lossy image compression with conditional diffusion models. In *Thirty-seventh Conference on Neural Information Processing Systems*, 2023. URL <https://openreview.net/forum?id=QIBpzaDCAv>.
- Lvmin Zhang, Anyi Rao, and Maneesh Agrawala. Adding conditional control to text-to-image diffusion models. In *Proceedings of the IEEE/CVF International Conference on Computer Vision*, pp. 3836–3847, 2023.
- Richard Zhang, Phillip Isola, Alexei A Efros, Eli Shechtman, and Oliver Wang. The unreasonable effectiveness of deep features as a perceptual metric. In *Proceedings of the IEEE Conference on Computer Vision and Pattern Recognition*, pp. 586–595, 2018.
- Yinhao Zhu, Yang Yang, and Taco Cohen. Transformer-based transform coding. In *International Conference on Learning Representations*, 2021.

A MATHEMATICAL DETAILS

Derivation of Eq. (4). First, according to Eq. (2), \mathbf{z}_{n-1} can be sampled as:

$$\mathbf{z}_{n-1} = \sqrt{\bar{\alpha}_{n-1}}(\mathbf{z}_0 + \eta_{n-1}\mathbf{e}) + \sqrt{1 - \bar{\alpha}_{n-1}}\epsilon_{n-1} \quad (12)$$

$$= \sqrt{\bar{\alpha}_{n-1}}\mathbf{z}_0 + \sqrt{\bar{\alpha}_{n-1}}\eta_{n-1}\mathbf{e} + \underbrace{\sqrt{1 - \bar{\alpha}_{n-1}}\epsilon_{n-1}}_{\sim \mathcal{N}(0, (1 - \bar{\alpha}_{n-1})\mathbf{I})}, \quad (13)$$

where $\epsilon_{n-1} \sim \mathcal{N}(0, \mathbf{I})$. Second, for \mathbf{z}_n defined in Eq. (2) and \mathbf{z}_{n-1} defined in Eq. (3), we have:

$$\mathbf{z}_{n-1} = k_n\mathbf{z}_0 + m_n\mathbf{z}_n + \sigma_n\epsilon \quad (14)$$

$$= k_n\mathbf{z}_0 + m_n(\sqrt{\bar{\alpha}_n}(\mathbf{z}_0 + \eta_n\mathbf{e}) + \sqrt{1 - \bar{\alpha}_n}\epsilon_n) + \sigma_n\epsilon \quad (15)$$

$$= (k_n + m_n\sqrt{\bar{\alpha}_n})\mathbf{z}_0 + m_n\sqrt{\bar{\alpha}_n}\eta_n\mathbf{e} + \underbrace{m_n\sqrt{1 - \bar{\alpha}_n}\epsilon_n + \sigma_n\epsilon}_{\sim \mathcal{N}(0, (m_n^2(1 - \bar{\alpha}_n) + \sigma_n^2)\mathbf{I})}, \quad (16)$$

where $\epsilon_n \sim \mathcal{N}(0, \mathbf{I})$ and $\epsilon \sim \mathcal{N}(0, \mathbf{I})$. By combining Eq. (13) and Eq. (16), we obtain the following equations:

$$\begin{cases} \sqrt{\bar{\alpha}_{n-1}} = k_n + m_n\sqrt{\bar{\alpha}_n}, \\ \sqrt{\bar{\alpha}_{n-1}}\eta_{n-1} = m_n\sqrt{\bar{\alpha}_n}\eta_n, \\ 1 - \bar{\alpha}_{n-1} = m_n^2(1 - \bar{\alpha}_n) + \sigma_n^2. \end{cases} \quad (17)$$

Note that, referring to DDIM (Song et al., 2021), we set $\sigma_n = 0$ for simplicity. By solving Eq. (17), we have:

$$k_n = \sqrt{\bar{\alpha}_{n-1}} - \sqrt{\frac{1 - \bar{\alpha}_{n-1}}{1 - \bar{\alpha}_n}}\sqrt{\bar{\alpha}_n}, \quad m_n = \sqrt{\frac{1 - \bar{\alpha}_{n-1}}{1 - \bar{\alpha}_n}}, \quad \frac{\eta_n}{\eta_{n-1}} = \frac{\sqrt{1 - \bar{\alpha}_n}/\sqrt{\bar{\alpha}_n}}{\sqrt{1 - \bar{\alpha}_{n-1}}/\sqrt{\bar{\alpha}_{n-1}}}. \quad (18)$$

Therefore, η_n can be defined as:

$$\eta_n = \lambda \frac{\sqrt{1 - \bar{\alpha}_n}}{\sqrt{\bar{\alpha}_n}}, \quad (19)$$

where we set $\lambda = \frac{\sqrt{\bar{\alpha}_N}}{\sqrt{1 - \bar{\alpha}_N}}$ to ensure $\eta_N = 1$.

Derivation of Eq. (8). Substituting Eq. (6) into Eq. (7), we have:

$$\|\mathbf{z}_0 - \hat{\mathbf{z}}_0\|_2^2 = \left\| \left(\frac{\mathbf{z}_n}{\sqrt{\bar{\alpha}_n}} - \frac{\sqrt{1 - \bar{\alpha}_n}}{\sqrt{\bar{\alpha}_n}}\tilde{\epsilon}_n \right) - \left(\frac{\mathbf{z}_n}{\sqrt{\bar{\alpha}_n}} - \frac{\sqrt{1 - \bar{\alpha}_n}}{\sqrt{\bar{\alpha}_n}}\epsilon_\theta(\mathbf{z}_n, \mathbf{c}, n) \right) \right\|_2^2 \quad (20)$$

$$= \left\| \frac{\sqrt{1 - \bar{\alpha}_n}}{\sqrt{\bar{\alpha}_n}}\tilde{\epsilon}_n - \frac{\sqrt{1 - \bar{\alpha}_n}}{\sqrt{\bar{\alpha}_n}}\epsilon_\theta(\mathbf{z}_n, \mathbf{c}, n) \right\|_2^2 \quad (21)$$

$$= \frac{1 - \bar{\alpha}_n}{\bar{\alpha}_n} \|\tilde{\epsilon}_n - \epsilon_\theta(\mathbf{z}_n, \mathbf{c}, n)\|_2^2 \quad (22)$$

B ADDITIONAL EXPERIMENTAL DETAILS

Evaluation of third-party models. For VVC (Bross et al., 2021), we used the reference software VTM-23.0² with intra configuration. The quality factor was selected from the set {41, 43, 45, 47, 49, 52}. To compare HiFiC (Mentzer et al., 2020) at extremely low bitrates, we utilized its PyTorch implementation³ and retrained the model to achieve higher compression ratios, enabling a more direct comparison with our proposed method. For PerCo (Careil et al., 2024), since the official source codes and models are not available, we used a reproduced version⁴ as a substitute, which employs stable diffusion as the latent diffusion model. For MS-ILLM (Muckley et al., 2023), VQIR (Wei et al., 2024), Text+Sketch (Lei et al., 2023) and DiffeIC (Li et al., 2024b), we used the publicly released checkpoints from their GitHub repositories, and used them for evaluation with the provided code.

²https://vcgit.hhi.fraunhofer.de/jvet/VVCSoftware_VTM/-/tree/VTM-23.0

³<https://github.com/Justin-Tan/high-fidelity-generative-compression>

⁴<https://github.com/Nikolai10/PerCo/tree/master>

C ADDITIONAL EXPERIMENTAL RESULTS

Quantitative comparisons on the Tecnick and Kodak datasets. We present the performance of the proposed and compared methods on the Tecnick and Kodak datasets in Fig. 9 and Fig. 10, respectively. The proposed RDEIC achieves state-of-the-art perceptual performance and significantly outperforms other diffusion-based methods in terms of distortion metrics. Since the Kodak dataset is too small to reliably calculate FID and KID scores, we do not report these results for this dataset.

More qualitative results. Fig. 11 and Fig. 12 provide more qualitative comparisons between the proposed RDEIC and other methods. These comparisons reveal the superiority of RDEIC in terms of both fidelity and realism.

Smoothness-sharpness trade-off. As shown in Fig. 13, Fig. 14, and Fig. 15, we control the balance between smoothness and sharpness by adjusting the parameter λ_s , which regulates the amount of high-frequency details introduced into the reconstructed image.

D LIMITATIONS

Using pre-trained stable diffusion may generate hallucinated lower-level details at extremely low bitrates. For instance, as shown in Fig. 8, the generated human faces appear realistic but are inaccurate, which may lead to a misrepresentation of the person’s identity. Furthermore, although the proposed RDEIC has shown promising compression results, the potential of incorporating a text-driven strategy has not yet been explored within our framework. We leave detailed study of this to future work.

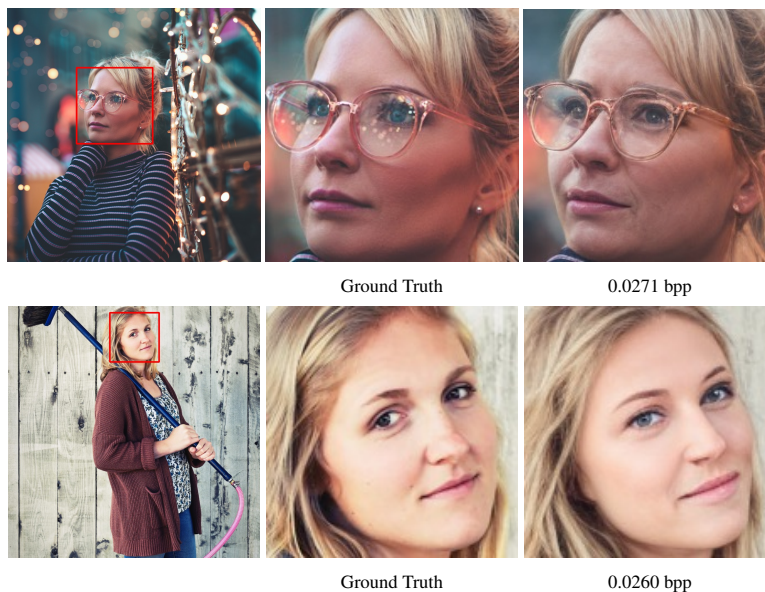


Figure 8: Faces generated at extremely low bitrates.

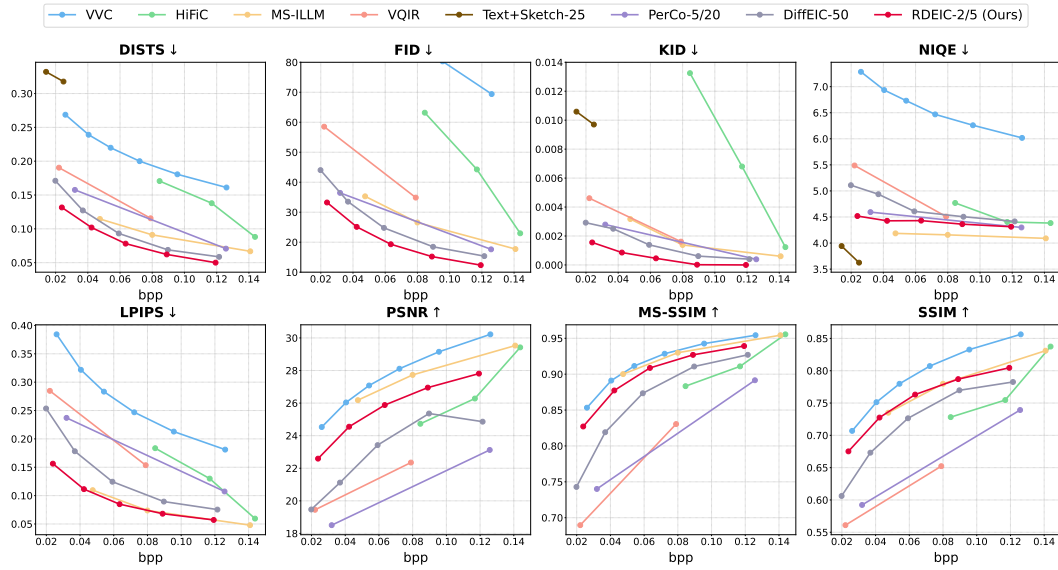


Figure 9: Quantitative comparisons with state-of-the-art methods on the Tecnick dataset.

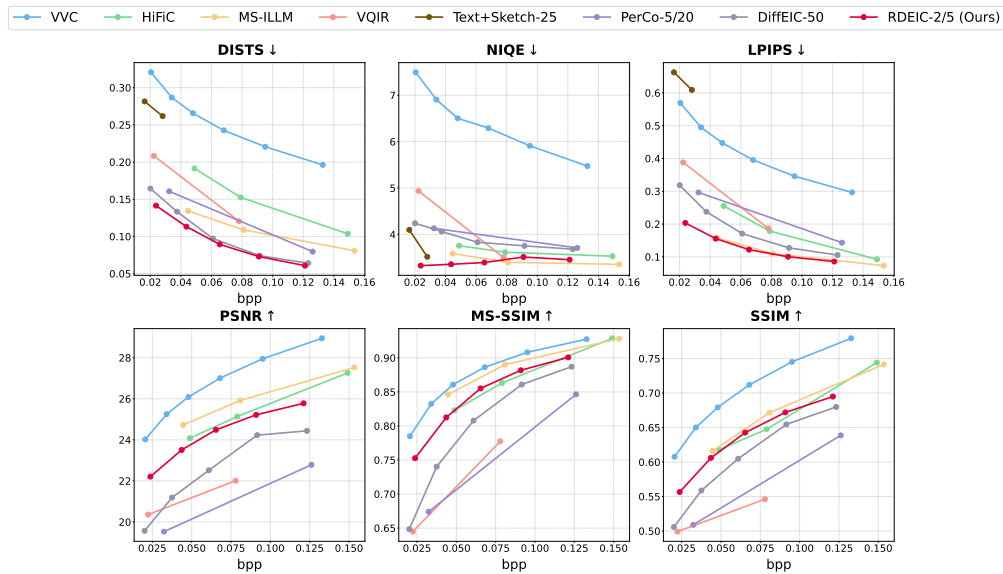


Figure 10: Quantitative comparisons with state-of-the-art methods on the Kodak dataset.

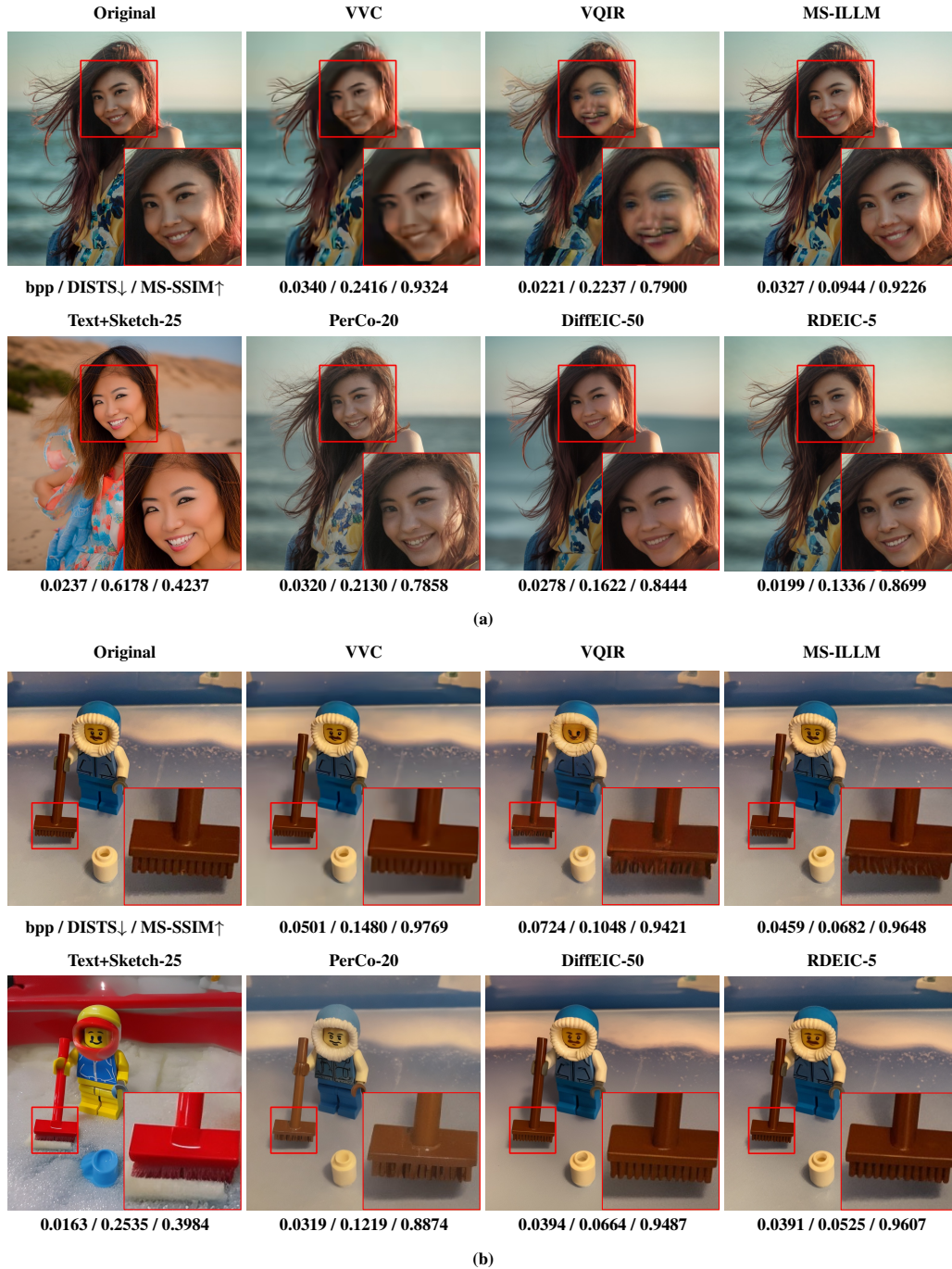


Figure 11: More qualitative comparisons between RDEIC and other methods.



Figure 12: More qualitative comparisons between RDEIC and other methods.

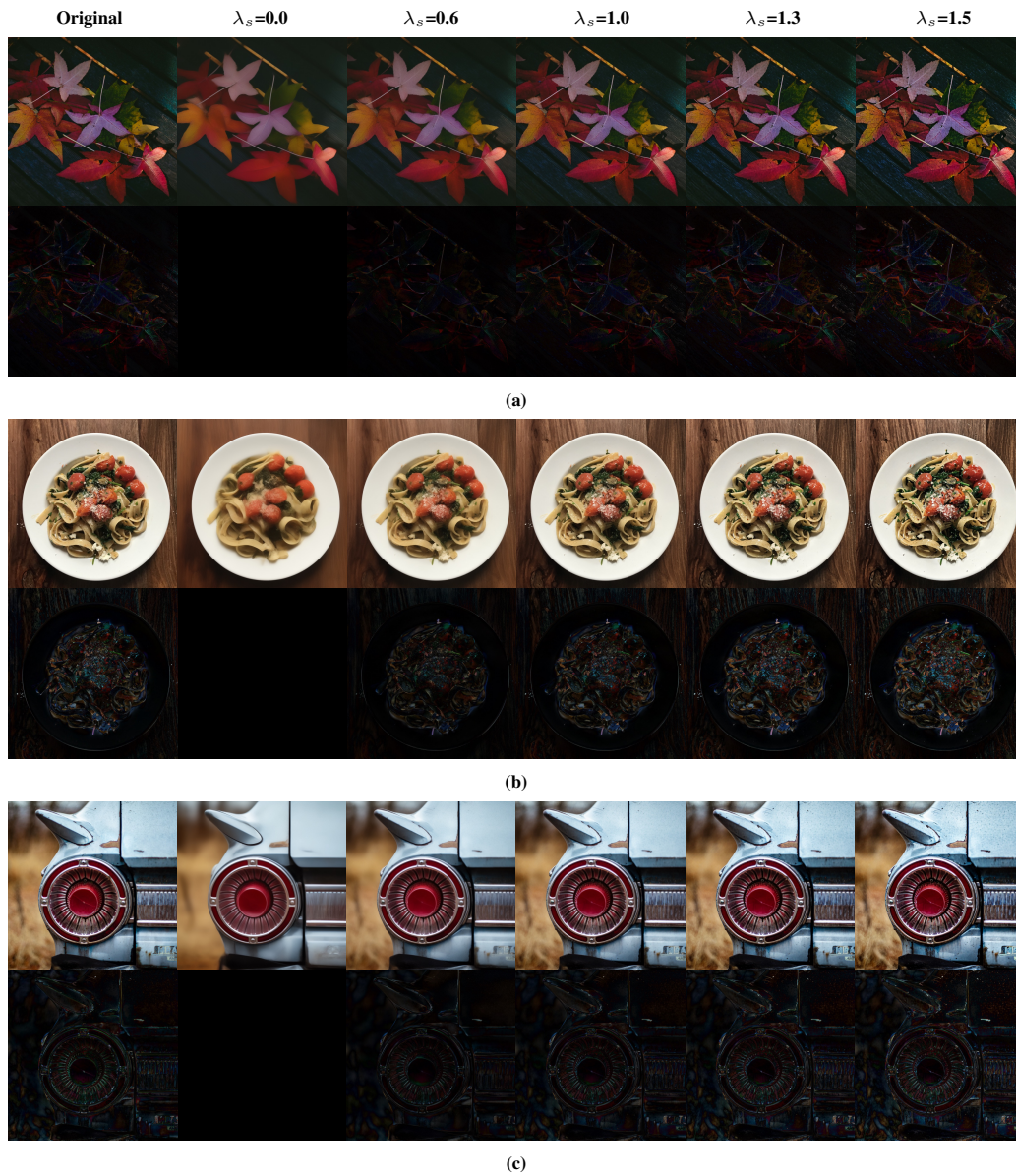


Figure 13: More results regarding the balance between smoothness and sharpness.



Figure 14: More results regarding the balance between smoothness and sharpness.

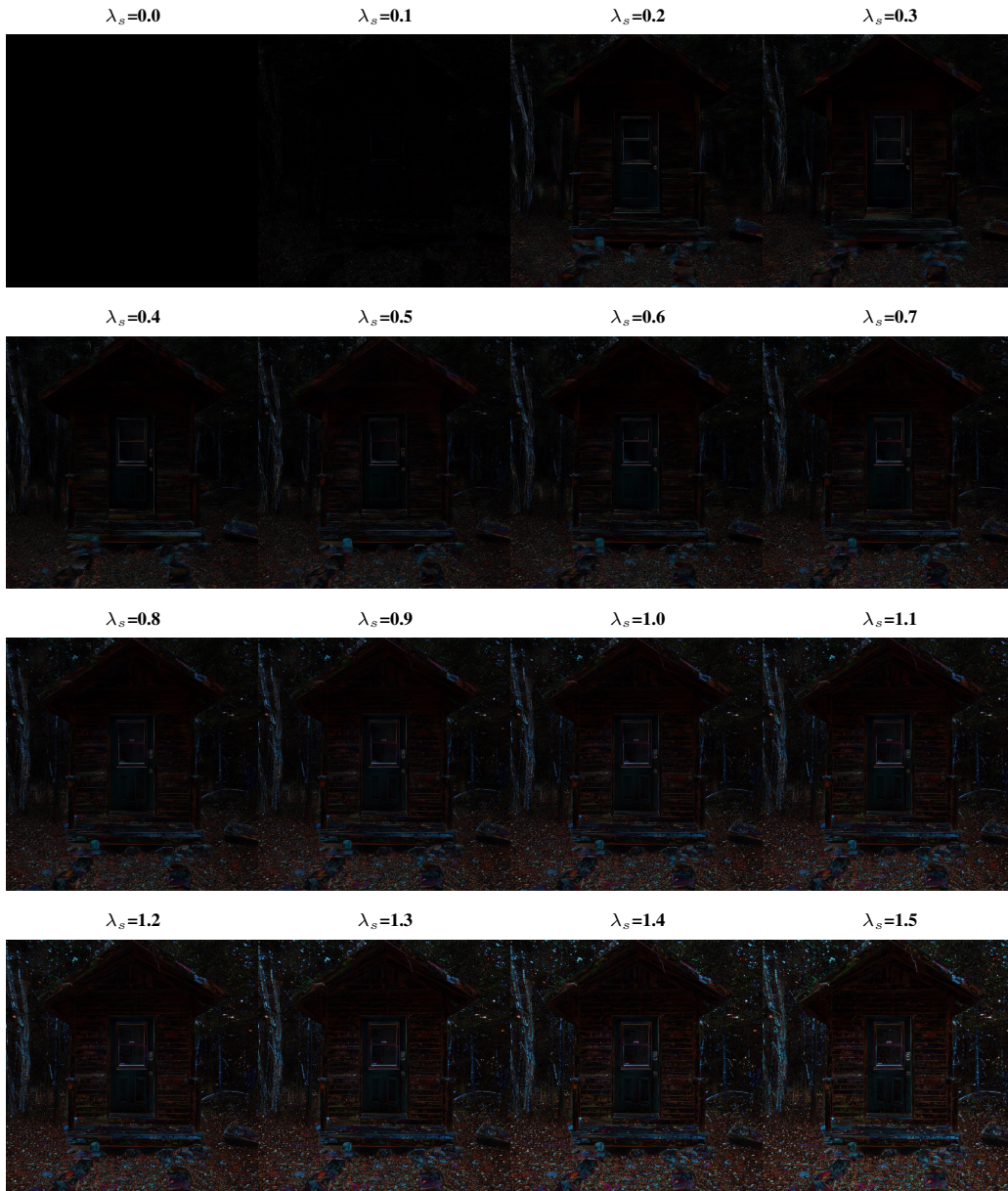


Figure 15: More results regarding the balance between smoothness and sharpness.